Published in final edited form as:
IEEE Trans Biomed Eng. 2010 April ; 57(4): 953–959. doi:10.1109/TBME.2009.2033464.

Biomechanical Properties of *In Vivo* Human Skin From Dynamic Optical Coherence Elastography

Xing Liang and
Department of Electrical and Computer Engineering, Beckman Institute for Advanced Science and Technology, University of Illinois at Urbana-Champaign, Urbana, IL 61801 USA

Stephen A. Boppart [Senior Member, IEEE]
Department of Electrical and Computer Engineering, Bioengineering, and Medicine, Beckman Institute for Advanced Science and Technology, University of Illinois at Urbana-Champaign, Urbana, IL 61801 USA

Xing Liang: xliang6@illinois.edu; Stephen A. Boppart: boppart@illinois.edu

Abstract

Dynamic optical coherence elastography is used to determine *in vivo* skin biomechanical properties based on mechanical surface wave propagation. Quantitative Young's moduli are measured on human skin from different sites, orientations, and frequencies. Skin thicknesses, including measurements from different layers, are also measured simultaneously. Experimental results show significant differences among measurements from different skin sites, between directions parallel and orthogonal to Langer's lines, and under different skin hydration states. Results also suggest surface waves with different driving frequencies represent skin biomechanical properties from different layers in depth. With features such as micrometer-scale resolution, noninvasive imaging, and real-time processing from the optical coherence tomography technology, this optical measurement technique has great potential for measuring skin biomechanical properties in dermatology.

Index Terms

Biomechanical properties; elastography; optical coherence tomography (OCT); skin

I. Introduction

Biomechanical properties of skin are of great importance as they contribute to or are responsible for skin health and disease, structural integrity, cosmesis, and aging. Early studies on human skin biomechanical properties began in the 19th century [1], which mainly focused on skin mechanical anisotropy. From this realized significance, further studies and investigations were conducted on skin biomechanical properties in the fields of skin aging [2], [3], plastic surgery [4], [5], sun exposure and skin cancer [6], [7], and cosmetics [8], [9]. With aging or pathological changes in human skin, thicknesses measurements and mechanical properties will vary for different layers of skin, and at regionally distinct sites,

Correspondence to: Stephen A. Boppart, boppart@illinois.edu.

Additional information can be found at http://biophotonics.illinois.edu.

Color versions of one or more of the figures in this paper are available online at http://ieeexplore.ieee.org.

making quantitative measurements more important for diagnosis and for monitoring of interventions.

A number of methods have been used for measuring skin mechanical properties. For example, ultrasound was used to determine skin thicknesses and mechanical properties *in vivo* [10]. A tangential traction method was used to determine the biomechanics of fingerpad tissue *in vivo* [11]. Young's modulus, initial stress, and index of nonelasticity of skin were characterized using a mechanical model under suction [12]. A twistometer was used to determine skin-related mechanical properties of human skin *in vivo* [3]. Strain–stress relationships were studied to determine the role of elastin in the mechanical properties of skin [13]. Wave propagation methods were also used to determine skin viscoelastic properties [14], [15]. A single-axis extension method was used to test the viscoelastic behavior of skin *in vivo*, using a mechanical model [16]. For all these studies, cross-sectional imaging-based techniques have become popular because of their added ability for high-speed, high-resolution measurements of thickness, morphological changes in disease, and assessment of biomechanical properties.

Among the imaging modalities, optical coherence tomography (OCT) has shown great potential in the field of dermatology based on its micrometer-scale resolution, millimeter-scale penetration, and noninvasive 3-D imaging ability [17], [18]. The principle of OCT is to depth-resolve optical scattering variations within tissue using interferometric techniques, in which the axial resolution is determined by the coherence length of the light source, and the transverse resolution is determined by the spot size of the incident beam. The imaging penetration of OCT in skin can be up to 1.5 mm, depending on the wavelengths of the light sources [19], and a new interferometric synthetic aperture microscopy technique can computationally improve the OCT transverse resolution and imaging depth-of-field simultaneously [20]. OCT has been successfully applied in dermatology and compared with other imaging modalities, such as ultrasound [21], [22]. In dermatology, polarization-sensitive OCT can reveal the birefringence properties of skin and can be used to image changes during thermal injury [23], [24].

Optical coherence elastography (OCE) is a novel technology used to determine tissue biomechanical properties and is based on *in vivo* OCT imaging. In OCE, mechanical stimulations are applied to biological tissues with simultaneous OCT scanning to detect cross-sectional biomechanical properties of the sample [25]. With cellular-level resolution and several millimeters of imaging penetration, OCE has the unique ability to noninvasively measure tissue biomechanical properties *in vivo*. OCE has been applied in intravascular imaging [26], [27], atherosclerotic tissue imaging [28], and imaging of engineered and developing tissues [29]. Phase-resolved OCE methods have also been successfully used for measuring tissue mechanical properties with increased sensitivity over amplitude-based methods [30], [31]. Our recent work demonstrated the feasibility of dynamic OCE for measuring and mapping biomechanical properties of tissues based on dynamic internal and external mechanical wave excitations and solutions to wave equations [32], [33]. In this paper, we focus on using the dynamic OCE technique to measure skin biomechanical properties *in vivo*. Quantitative *in vivo* measurements of Young's moduli in human skin were obtained.

II. Materials and Method

A. Tissue Phantom Preparation

Multilayer tissue phantoms were used to calibrate the measurements of mechanical properties by the OCE system because of their similar optical scattering and biomechanical properties to human tissues. Silicone-based tissue phantoms were used due to their

permanence and the ability to vary stiffness [34]. Phantoms were prepared from pure polydimethylsiloxane fluid (50 cSt viscosity, ClearCo, Inc.), a room temperature vulcanizing silicone, and its associated curing agent (General Electric RTV-615A and B, respectively, Circuit Specialists, Inc.). Different concentration ratios of these three ingredients were used to obtain layer structures with different stiffness and thickness in the samples. Titanium dioxide powder (Sigma–Aldrich, #224227, mean size 1 μm and maximum size 5 μm) were embedded with a concentration of 1 mg/g in the tissue phantoms to function as optical scatterers for OCE imaging. The phantom solutions were mixed thoroughly in an ultrasonicator for 30 min at room temperature, and then poured into 9 cm plastic Petri dishes. Different layers of samples with different stiffness and thickness were separately fabricated after the curing process of the previous layer, which included curing at 80 °C for 8 h, and subsequently, at room temperature for 24 h.

B. Human Subject Measurements

All *in vivo* experiments were done on the skin of a healthy male volunteer under room temperature and humidity. Informed consent was obtained from the subject. The sites of skin were chosen as relatively flat regions from the volar forearm, dorsal forearm, and palm.

C. OCE System

A spectral-domain OCT system with a center wavelength of 800 nm and a bandwidth of 100 nm was used in this study, providing an axial resolution of about 3 μm in the skin. A 12.5-mm-diameter and 40-mm-focal length lens was used in the sample arm to provide a transverse resolution of 13 μm. The average power incident on the skin was 5 mW. A line camera was used to detect the spectral interference signal with an acquisition rate of 25 kHz. A mechanical wave driver (SF-9324, PASCO scientific, Roseville, CA) was used for external mechanical excitation and the spectral-domain OCT system was used for detection of surface wave propagation on the skin. The mechanical wave driver was synchronized with the OCT system and sinusoidal waves were generated on the skin surface. A schematic of the experimental setup is shown in Fig. 1. The initial distance between the OCT sample arm beam and the mechanical wave driver was chosen arbitrarily to be 16 mm. An M-mode OCT image was recorded at the first position, and then the sample arm beam was moved away from the mechanical wave driver at a step distance of 2 mm, before the next image was taken. The step distance was chosen to be less than one-half the wavelength of the surface wave for all frequencies to ensure the accuracy of the wave velocity calculation. Six step-imaging positions were made for averaging data for each measurement. Phase data from OCT images were used for detecting the skin displacement.

D. Analysis Algorithm for Skin Mechanical Properties

The skin was modeled as an infinite elastic homogeneous layer as shown in Fig. 2. Waves generated by the harmonic excitation were polarized in the x–z plane and propagated in the x-direction. The wave propagation was governed by the differential equations

$$\frac{\partial^2\varphi}{\partial x^2}+\frac{\partial^2\varphi}{\partial z^2}=\frac{1}{c_L^2}\frac{\partial^2\varphi}{\partial t^2} \quad (1)$$

and

$$\frac{\partial^2 H_z}{\partial x^2}+\frac{\partial^2 H_z}{\partial z^2}=\frac{1}{c_T^2}\frac{\partial^2 H_z}{\partial t^2} \quad (2)$$

where φ and H_z are potentials in the x- and z-directions, respectively, and c_L and c_T are wave velocities for the longitudinal and shear directions, respectively. The solution for the displacement in the z-direction can be expressed as

$$u_z=\mathrm{Re}\left(\frac{\partial\varphi}{\partial z}+\frac{\partial H_z}{\partial x}\right)=(Ae^{-qz}-2sqe^{-sz})\cos(k_R x-\omega t) \quad (3)$$

where A, s, and q are parameters for calculation, and k_R is the wavenumber of the surface wave propagating on the surface of the skin. By recording the displacements in the z-direction for two positions x_1 and x_2 in the x-direction from OCT, the sinusoidal phase delay can be determined by

$$\Delta\phi=k_R(x_1-x_2). \quad (4)$$

Thus, by using (4), the surface wave velocity can be calculated as $v_R = \omega D/\Delta\phi$, where ω is the driving angular frequency and $D = x_1 - x_2$. In the experiments, peaks of propagating surface waves averaged over the range of interest were recorded for each location to calculate the surface wave velocity.

Surface wave velocity is an important parameter for material mechanical properties and by which Young's modulus can be determined, using the relationship of

$$E=\rho v_R^2(2.618+1.332\nu) \quad (5)$$

where ν is Poisson's ratio for skin and ρ is the mass density for skin [35]. By this method, we can quantitatively measure the Young's moduli of *in vivo* human skin by OCE.

E. Cutometer Measurements

Measured Young's moduli of *in vivo* skin were verified using a commercial instrument (Cutometer MPA 580, Courage Khazaka Electronic, Koln, Germany). The Cutometer measurements were conducted after the OCE measurements, using a 2-mm Cutometer probe fixed on the same skin area by a double-sided adhesive ring. The Cutometer experiments were measured with a pressure of 450 mbar. On-time, off-time, and repetition numbers were 5 s, 3 s, and 3, respectively. The parameter Ur/Uf was used to represent the skin elastic moduli [36], and compared with the Young's moduli results measured by OCE.

III. Results

A. Skin Thickness Measurements by OCT

Cross-sectional brightness mode (B-mode) OCT images for skin sites on the volar forearm, dorsal forearm, and palm are shown in Fig. 3. From the B-mode images, structural features of human skin can be clearly discerned. For example, the skin over the palm has a thicker stratum corneum, shown in Fig. 3(c). Optical thickness of skin can be determined by B-mode OCT images. Physical thickness of the skin can then be simply estimated, using the optical thickness divided by the refractive indices. By using refractive indexes of $n = 1.53$ and 1.39 for the stratum corneum and epidermis, respectively [37], the physical thickness of skin layers at different sites can be determined [see Fig. 3(d)]. At sites other than the palm or sole, where the stratum corneum is thick, the stratum corneum thickness can be difficult to measure with OCT because the thickness is comparable to the coherence length (axial resolution, 2–5 μm) of the OCT system.

B. Skin Young's Moduli Measurements by OCE

For OCE measurements, motion mode (M-mode, repetitive axial depth-scans into the tissue, acquired at a fixed transverse position over time) OCT images were taken at one transverse position of the skin. In Fig. 4(a), the arrow denotes the fixed location of the OCT beam, and Fig. 4(b) and (c) denote the amplitude and phase data of the M-mode OCT image at this position, respectively. By averaging over the range of interest [dotted line range in Fig. 4(c)], the phase of the optical data can be plotted, as shown in Fig. 4(d). The envelope ripples in Fig. 4(d) are due to very subtle motion artifacts, which will not affect the measurement results because our calculations are based on sinusoidal phase differences between different measurement positions.

Using the sinusoidal phase changes from different positions of the skin measured by OCE, along with wave equation algorithms, we can calculate surface wave velocities, and subsequently, the Young's moduli of human skin. The results of measured Young's moduli by OCE in this study are based on an average of six measurements and the error bars denote standard deviations. Fig. 5(a) shows the results measured by OCE from different sites on human skin. All measurements were conducted approximately orthogonal to Langer's lines and with a driving frequency of 50 Hz. The Young's moduli from the volar forearm, dorsal forearm, and palm are 101.180, 68.678, and 24.910 kPa, respectively.

As shown in Fig. 5(b), the OCE-measured Young's moduli from different sites correspond well with the elasticity measured by the Cutometer MPA 580, which is a well-characterized commercial skin stiffness measurement device. Calculations assumed a skin mass density of 1.02 g/cm^2 and a Poisson's ratio of 0.5.

C. Frequency Dependence of OCE Measurements

Fig. 6 shows the OCE measurements of skin mechanical properties with different driving frequencies and under different hydration conditions. Skin measurements were acquired from the volar forearm of the volunteer. Skin hydration conditions include hydrated, dehydrated, and normal. A hydrated skin condition was produced by soaking normal skin in a water bath for 20 min, followed by a topical application of glycerin for 10 min. A dehydrated skin condition was produced by passing heated air from a commercial hair dryer over normal skin for 30 min. We can observe from Fig. 6 that normal skin has a Young's modulus of 101.20 kPa under a driving frequency of 50 Hz. This value decreases when the driving frequency increases. The Young's modulus increases again with a driving frequency of more than 300 Hz. The hydrated skin exhibited a smaller Young's modulus under a driving frequency of 50 Hz, and when the driving frequency increased, the measured Young's moduli increased as well, with larger values than the normal skin. The dehydrated skin exhibited the largest Young's modulus under a driving frequency of 50 Hz, and the value decreased dramatically with increasing frequency, with a Young's moduli comparable with the normal skin.

D. OCE Measurements on Skin Tissue Phantoms

Similar OCE experiments were also performed on multilayer tissue phantoms. Three different tissue phantoms were fabricated with different number, thickness, and stiffness of layers, as shown in Fig. 7. Driving frequencies for these experiments were limited to less than 500 Hz to clearly differentiate the surface wave propagation in time. We observed from Fig. 7 that phantom 1 has a relatively high measured Young's modulus under low driving frequency, and the value decreases until the driving frequency reaches 500 Hz. For phantom 2, the measured Young's modulus decreases as the driving frequency increases. For phantom 3, the measured Young's modulus is low under 50 Hz driving frequency, but the

value increases at a driving frequency of 100 Hz and increases further at a driving frequency of 400 Hz.

E. Skin Directionality Measured by OCE

Fig. 8 shows the measured OCE results acquired from different directions along the surface of human skin. The results were measured on the volar forearm, parallel and orthogonal to Langer's lines, and with driving frequencies of 50 and 600 Hz. Langer's lines describe the patterns of biomechanical anisotropy in human skin. Directions within skin and along (parallel to) Langer's lines have the least flexibility (highest Young's modulus) [1]. We chose the volar forearm for these measurements because the Langer's lines are easily defined at this site to be parallel to the long axis of the arm [38].

From Fig. 8, we can see that the measured Young's modulus parallel to Langer's lines can be differentiated from the Young's modulus from the orthogonal direction under a driving frequency of 50 Hz. However, when the driving frequency is increased to 600 Hz, the measured Young's modulus parallel to Langer's lines is significantly larger and different than from the direction orthogonal to Langer's lines, with a ratio of 2.21. These findings correspond well with the anisotropy trend previously reported [37]. From these results, we observe that OCE measurements show a larger difference in the anisotropy of skin mechanical properties under high driving frequency rather than at lower frequencies under 50 Hz. These results suggest the ability to resolve depth-dependent biomechanical properties in human skin based on frequency-dependent driving mechanical waves.

IV. Discussion

This study reports biomechanical measurements by dynamic OCE on *in vivo* human skin and on multilayer tissue phantoms with quantitative results of measured Young's moduli. The results show that the measured Young's moduli are site, direction, and frequency dependent. Furthermore, different conditions such as hydrated or dehydrated skin also showed significant differences between measured results.

The frequency-dependent results from dynamic OCE measurements on human skin and multilayer tissue phantoms are significant. From the literature, it was found that Young's moduli measured with different frequencies correspond to the skin stiffness from different depths [39]. At a low surface wave driving frequency, dynamic skin mechanical properties were believed to be primarily due to the outer layer (stratum corneum), while at higher frequencies, the properties were believed to be dominated by the deeper layer (dermis). Based on this theory, the results can be understood as the following. For normal skin (as in Fig. 6), the measured Young's modulus is 101.20 kPa under a 50 Hz driving frequency, which represents the mechanical properties of the stratum corneum. The measured Young's modulus decreases until a driving frequency of 200 Hz and increases again, implying that the epidermis layer has a lower stiffness than the dermis layer. For the hydrated skin, the measured Young's modulus is only 23.01 kPa under a 50 Hz driving frequency, which denotes the stratum corneum has been softened by the hydrating process. However, the hydrating process tends to increase the stiffness of the skin in the epidermis and dermis layers, since the measured Young's moduli are increasing when the driving frequency increases. From the literature, the hydration process does affect skin mechanical properties, but whether the process makes the deeper skin layers stiffer or less stiff, is all subject dependent [40]. For the dehydrated skin, the measured Young's modulus is 300.41 kPa under a 50 Hz driving frequency, but for higher frequencies, the measured Young's moduli remain similar to those of normal skin. These findings support the physiology that the outer stratum corneum serves to protect the deeper skin layers against dehydrating conditions.

The relationship between driving frequency and skin measurement depth was verified by experiments on multilayer tissue phantoms (as in Fig. 7). Phantom 1 mimicked human skin with four layers. The first layer has the largest Young's modulus of about 100 kPa, while the second layer has a lower value of 25 kPa. The third layer mimics the dermal layer in human skin and has a rather high Young's modulus of 75 kPa, while the fourth layer is very soft (Young's modulus of 8 kPa), playing the role of the hypodermal adipose layer of skin. The experimental results show a Young's modulus of about 50 kPa below 100 Hz, denoting the first layer, and a rather low Young's modulus between 200 and 400 Hz, denoting the second layer. The measurements from the third layer under a driving frequency of 500 Hz indicate an increase in the measured Young's modulus. The results indicate a 500 Hz driving wave reaches a depth around 250 μm in phantom 1. Results from phantoms 2 and 3 also follow the trends pertaining to layer thickness and stiffness within the phantoms. We recognize that these multilayer tissue phantoms do not fully replicate the complex biomechanical structures and properties within living skin. Rather, their use is intended to validate the frequency-dependent depth measurements acquired by this method. Although this dynamic OCE method is not capable of decoupling mechanical properties from each layer, it is applicable to measuring biomechanical properties in human skin layers, and also suitable for more general multilayer structures.

Skin anisotropy measurements by dynamic OCE also support the findings mentioned previously. Under a driving frequency of 50 Hz, the Young's moduli between directions parallel and orthogonal to Langer's lines are comparable, but under a driving frequency of 600 Hz (corresponding to depths within the dermis), the measured Young's modulus of skin parallel to Langer's lines is significantly larger than the orthogonal value. This is likely due to the fact that anisotropic microstructure like collagen is located in the deeper dermal layer of skin, and not in the more superficial layers. However, this frequency–depth relationship is only relative because factors, such as thickness, stiffness, binding, and complex boundary conditions all contribute in ways that are not currently understood.

One assumption used in this study is that the skin can be modeled as pure elastic strips. From our experimental results, this assumption is valid because no significant decay in amplitude of surface wave propagation over distance was noticed within the range of amplitudes and frequencies used in this study. For specific experimental conditions, such as with a high-frequency driving wave, a viscoelastic mechanical model could be used for additional quantitative measurements [14], [41].

In this study, we report a dynamic OCE technique used to measure skin thickness and stiffness quantitatively. Skin layer thickness and Young's moduli have been measured quantitatively on human skin *in vivo* with a lab-based instrument. Direction-dependent and site-dependent mechanical properties were measured and resolved *in vivo* in human skin. Surface waves with different frequencies have been utilized to mechanically drive skin and Young's moduli have been determined based on solutions to wave equations. A depth and driving frequency dependence theory on surface wave propagation can be used to explain the results, which were also verified by results on polymer tissue phantoms. Inheriting capabilities from OCT, such as micrometer-scale resolution, noninvasive imaging, and real-time processing, this OCE technique has been successfully applied to measuring skin biomechanical properties *in vivo* with features including skin thickness, skin mechanical anisotropy, and depth-dependent variations. Compared with other previously used imaging technologies on human skin measurements such as ultrasound imaging, OCE can differentiate thickness with a resolution of several micrometers, which is critical for resolving different skin layers and their properties. With state-of-the-art OCT hand-held probes [18], this dynamic OCE technique has potential applications in clinical dermatology, plastic surgery, and cosmetic skin assessment. This technique may also find application

where skin thickness and stiffness measurements are critical for interventions and devices, such as in transcutaneous microneedle applications [44]. Further studies are needed to refine the 3-D mechanical modeling algorithms and generate high-resolution 2-D or 3-D maps of the mechanical properties of human skin.

Acknowledgments

This work of S. A. Boppart was supported in part by the National Science Foundation under Grant BES 05-19920, in part by the National Institutes of Health under Grant National Institute of Biomedical Imaging and Bioengineering (NIBIB) R01 EB005221, and in part by the Roadmap Initiative under Grant NIBIB R21 EB005321.

The authors would like to thank Dr. H. Tu and E. J. Chaney for their laboratory assistance. This study was performed at the Beckman Institute for Advanced Science and Technology, University of Illinois at Urbana-Champaign.

References

1. Wilhelmi BJ, Bradon J, Blackwell SJ, Phillips LG. Langer's lines: To use or not to use. Plast Reconstr Surg. 1999; 104:208–214. [PubMed: 10597698]
2. Vogel HG. Directional variations of mechanical parameter in rat skin depending on maturation and age. J Invest Dermatol. 1981; 76:493–497. [PubMed: 7240796]
3. Escoffier C, de Rigal J, Rochefort A, Vasselet R, Leveque JL, Agache PG. Age-related mechanical properties of human skin: An *in vivo* study. J Invest Dermatol. 1989; 93:353–357. [PubMed: 2768836]
4. Jemec GB, Jemec B, Jemec BI, Serup J. The effect of superficial hydration on the mechanical properties of human skin *in vivo*: Implications for plastic surgery. Plast Reconstr Surg. 1990; 85:100–103. [PubMed: 2293715]
5. Lu WW, Ip WY, Jing WM, Holmes AD, Chow SP. Biomechanical properties of thin skin flap after basic fibroblast growth factor (bFGF) administration. Brit J Plast Surg. 2000; 53:225–229. [PubMed: 10738329]
6. Nishimori N, Edwards C, Pearse A, Matsumoto K, Kawai M, Marks R. Degenerative alterations of dermal collagen fiber bundles in photodamaged human skin and UV-irradiated hairless mouse skin: Possible effect on decreasing skin mechanical properties and appearance of wrinkles. J Invest Dermatol. 2001; 117:1458–1463. [PubMed: 11886509]
7. Moon JS, Oh CH. Solar damage in skin tumors: Quantification of elastotic material. Dermitology. 2001; 4:289–292.
8. Wissing SA, Muller RH. The influence of solid lipid nanoparticles on skin hydration and viscoelasticity—*In vivo* study. Eur J Pharm Biopharm. 2003; 56:67–72. [PubMed: 12837483]
9. Salter DC, McArthur HC, Crosse JE, Dickens AD. Skin mechanics measured *in vivo* using torsion: A new and accurate model more sensitive to age, sex and moisturizing treatment. Int J Cosmet Sci. 2007; 15:200–218. [PubMed: 19272125]
10. Diridollou S, Berson M, Vabre V, Black D, Karlsson B, Auriol F, Gregoire JM, Yvon C, Vaillant L, Gall Y, Patat F. An *in vivo* method for measuring the mechanical properties of the skin using ultrasound. Ultrasound Med Biol. 1997; 24:215–224. [PubMed: 9550180]
11. Wang Q, Hayward V. *In vivo* biomechanics of the fingerpad skin under local tangential traction. J Biomech. 2006; 40:851–860. [PubMed: 16682045]
12. Diridollou S, Black D, Lagarde JM, Gall Y, Berson M, Vabre V, Papat F, Vaillant L. Sex- and site-dependent variations in the thickness and mechanical properties of human skin *in vivo*. Int J Cosmet Sci. 2000; 22:421–435. [PubMed: 18503429]
13. Oxlund H, Manschot J, Viidik A. The role of elastin in the mechanical properties of skin. J Biomech. 1988; 21:213–218. [PubMed: 3379082]
14. Pereira JM, Mansour JM, Davis BR. Dynamic measurement of the viscoelastic properties of skin. J Biomech. 1991; 24:157–162. [PubMed: 2037615]
15. Kirkpatrick SJ, Duncan DD, Fang L. Low-frequency surface wave propagation and the viscoelastic behavior of porcine skin. J Biomed Opt. 2004; 9:1311–1319. [PubMed: 15568953]

16. Khatyr F, Imberdis C, Vescovo P, Varchon D, Lagarde JM. Model of the viscoelastic behaviour of skin *in vivo* and study of anisotropy. Skin Res Technol. 2004; 10:96–103. [PubMed: 15059176]
17. Huang D, Swanson EA, Lin CP, Schuman JS, Stinson WG, Chang W, Hee MR, Flotte T, Gregory K, Puliafito CA, Fujimoto JG. Optical coherence tomography. Science. 1991; 254:1178–1181. [PubMed: 1957169]
18. Pierce MC, Strasswimmer J, Park BH, Cense B, de Boer JF. Advances in optical coherence tomography imaging for dermatology. J Invest Dermatol. 2004; 123:458–463. [PubMed: 15304083]
19. Welzel J. Optical coherence tomography in dermatology: A review. Skin Res Technol. 2001; 7:1–9. [PubMed: 11301634]
20. Ralston TS, Marks DL, Carney PS, Boppart SA. Interferometric synthetic aperture microscopy. Nat Phys. 2007; 3:129–134.
21. Schmitt JM, Yadlowsky MJ, Bonner RF. Subsurface imaging of living skin with optical coherence microscopy. Dermatology. 1995; 191:93–98. [PubMed: 8520074]
22. Vogt M, Knuttel A, Hoffmann K, Altmeyer P, Ermert H. Comparison of high frequency ultrasound and optical coherence tomography as modalities for high-resolution and noninvasive skin imaging. Biomed Tech (Berl). 2003; 48:116–121. [PubMed: 12838793]
23. de Boer JF, Srinivas SM, Malekafzali A, Chen Z, Nelson JS. Imaging thermally damaged tissue by polarization sensitive optical coherence tomography. Opt Exp. 1998; 3:212–218.
24. Saxer CE, de Boer JF, Park BH, Zhao Y, Chen Z, Nelson JS. High-speed fiberbased polarization-sensitive optical coherence tomography of *in vivo* human skin. Opt Lett. 2000; 25:1355–1357. [PubMed: 18066215]
25. Schmitt JM. OCT elastography: Imaging microscopic deformation and strain of tissue. Opt Exp. 1998; 3:199–211.
26. Khalil AS, Chan RC, Chau AH, Bouma BE, Kaazempur MMR. Tissue elasticity estimation with optical coherence elastography: Toward mechanical characterization of *in vivo* soft tissue. Ann Biomed Eng. 2005; 33:1631–1639. [PubMed: 16341928]
27. Van Soest G, Mastik F, de Jong N, van der Steen AFW. Robust intravascular optical coherence elastography by line correlations. Phys Med Biol. 2007; 52:2445–2458. [PubMed: 17440245]
28. Rogowska J, Patel NA, Fujimoto JG, Brezinski ME. Optical coherence tomographic elastography technique for measuring deformation and strain of atherosclerotic tissues. Heart. 2004; 90:556–562. [PubMed: 15084558]
29. Ko HJ, Tan W, Stack R, Boppart SA. Optical coherence elastography of engineered and developing tissue. Tissue Eng. 2006; 12:63–73. [PubMed: 16499443]
30. Wang RK, Kirkpatrick SJ, Hinds H. Phase-sensitive optical coherence elastography for mapping tissue microstrains in real time. Appl Phys Lett. 2007; 90:164105-1–164105-3.
31. Kirkpatrick SJ, Wang RK, Duncan DD. OCT-based elastography for large and small deformations. Opt Exp. 2006; 14:11585–11597.
32. Liang X, Oldenburg AL, Crecea V, Chaney EJ, Boppart SA. Optical microscale mapping of dynamic biomechanical tissue properties. Opt Exp. 2008; 16:11052–11065.
33. Liang X, Orescanin M, Toohey KS, Insana MF, Boppart SA. Acoustomotive optical coherence elastography for measuring material mechanical properties. Opt Lett. 2009; 34:2894–2896. [PubMed: 19794759]
34. Pogue BW, Patterson MS. Review of tissue simulating phantoms for optical spectroscopy, imaging and dosimetry. J Biomed Opt. 2006; 11:041102-1–041102-16. [PubMed: 16965130]
35. Bayon A, Gascon F, Nieves FJ. Estimation of dynamic elastic constants from the amplitude and velocity of Rayleigh waves. J Acoust Soc Amer. 2005; 117:3469–3477. [PubMed: 16018451]
36. Cua AB, Wilhelm KP, Maiback HI. Elastic properties of human skin: Relation to age, sex and anatomical region. Arch Dermatol Res. 1990; 282:283–288. [PubMed: 2221979]
37. Agache, P.; Humbert, P. Measuring the Skin. Berlin, Germany: Springer-Verlag; 2004. p. 748-750.
38. Langer K. On the anatomy and physiology of the skin I. The cleavability of the cutis. Brit J Plast Surg. 1978; 31:3–8. [PubMed: 342028]

39. Potts RO, Chrisman DA Jr, Buras EM Jr. The dynamic mechanical properties of human skin *in vivo*. J Biomech. 1983; 16:365–372. [PubMed: 6619155]

40. Hendriks FM, Brokken D, Oomens CWJ, Baaijens FPT. Influence of hydration and experimental length scale on the mechanical response of human skin *in vivo*, using optical coherence tomography. Skin Res Technol. 2004; 10:231–241. [PubMed: 15479446]

41. Jamison CE, Marangoni RD, Glaser AA. Viscoelastic properties of soft tissue by discrete model characterization. J Biomech. 1968; 1:33–46. [PubMed: 16329308]

42. Manschot JFM, Brakkee JM. The measurement and modelling of the mechanical properties of human skin *in vivo*: II. The model. J Biomech. 1986; 7:517–521. [PubMed: 3745224]

43. Barel, AO.; Lambrecht, R.; Clarys, R. Current Problems in Dermatology. Vol. 26. Basel, Switzerland: Karger; 1998. Skin Bioengineering Techniques and Applications in Dermatology and Cosmetology; p. 69-83.

44. Park JH, Yoon YK, Choi SO, Prausnitz MR, Allen MG. Tapered conical polymer microneedles fabricated using an integrated lens technique for transdermal drug delivery. IEEE Trans Bio-Med Eng. May; 2007 54(5):903–913.

Biographies

Xing Liang was born in Tianjin, China, in 1981. He received the B.S. and M.S. degrees in optics from Nankai University, Tianjin, China. He is currently working toward the Ph.D. degree with the Department of Electrical and Computer Engineering, Beckman Institute for Advanced Science and Technology, University of Illinois at Urbana-Champaign, Urbana, IL.

His current research includes investigating biomechanical properties at the tissue and cellular-level using optical coherence imaging techniques.

Mr. Liang is a Student Member of the Optical Society of America and the Biomedical Engineering Society.

Stephen A. Boppart (S'90–M'90–SM'06) was born in Harvard, IL, in 1968. He received the B.S. degree in electrical and bioengineering and the M.S. degree in electrical engineering, in 1990 and 1991, respectively, both from the University of Illinois at Urbana-Champaign, Urbana. He received the Ph.D. degree in electrical and medical engineering from the Massachusetts Institute of Technology, Cambridge, MA, in 1998, and the M.D. degree from Harvard Medical School, Boston, MA, in 2000. He completed residency

training in internal medicine from the University of Illinois at Urbana-Champaign, Urbana, in 2005.

Before beginning his doctoral work, he was a Research Scientist with the Air Force Laser Laboratory, Brooks Air Force Base, San Antonio, TX, where he was engaged in research on developing national (American National Standards Institute (ANSI)) and Air Force laser safety standards. In 2000. he joined the University of Illinois at Urbana-Champaign, Urbana, where he is currently a Professor with the Department of Electrical and Computer Engineering, Bioengineering and Medicine, Beckman Institute for Advanced Science and Technology, and the Head of the Biophotonics Imaging Laboratory, Beckman Institute for Advanced Science and Technology. He also holds an appointment as Leader of a campus-wide Imaging Initiative. He is the author or coauthor of more than 165 invited and contributed publications, and more than 400 invited and contributed presentations. He is the holder of more than 25 patents filed or pending. His research interests include the development of novel optical imaging technologies for biological and medical applications, with particular emphasis on translating these to clinical applications in cancer detection and diagnosis.

Dr. Boppart is a Fellow of the Optical Society of America and the International Society for Optical Engineering (SPIE), and a Member of the Society for Molecular Imaging, the Academy of Molecular Imaging, the American Association for the Advancement of Science, the American Association for Cancer Research, and the American Medical Association. In 2002, he was named as one of the top 100 Innovators in the world by the Technology Review Magazine for his research in medical technology, and in 2005, he received the IEEE Engineering in Medicine and Biology Society (EMBS) Early Career Achievement Award.

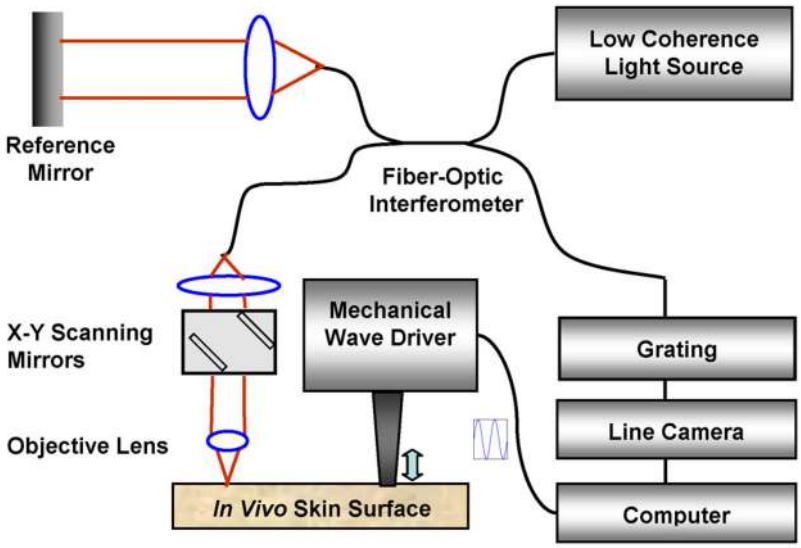

Fig. 1.

Schematic of OCE on skin. The mechanical wave driver is synchronized with the spectral domain OCT system and touching the skin surface with minimum force. The OCT sample arm optics is moved transversely across the skin surface.

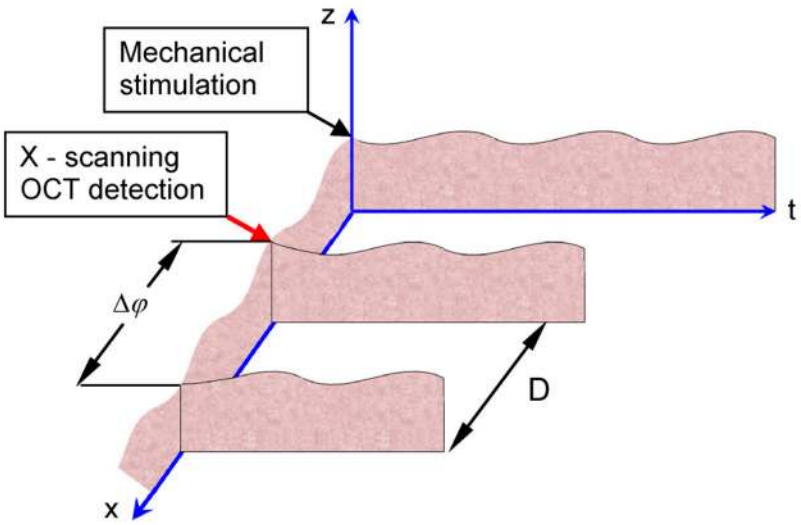

Fig. 2.

Schematic of surface wave propagation on skin. The mechanical wave driver moves along the *x*-axis by steps of $D = 2$ mm. At each step, an M-mode OCT image and phase shifts are recorded which are used to calculate surface wave propagation velocity.

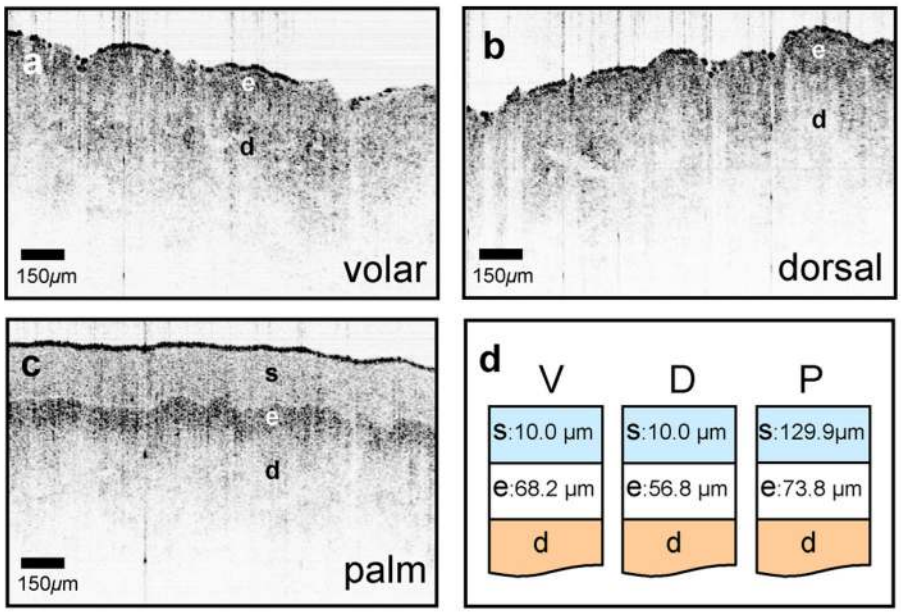

Fig. 3.

B-mode OCT images of human skin from different sites. Images were acquired from the (a) volar forearm, (b) dorsal forearm, and (c) palm. (d) Schematic showing OCT-measured thickness of different skin layers from (a) to (c). Abbreviations: e, epidermis; d, dermis; s, stratum corneum; V, volar forearm; D, dorsal forearm; P, palm.

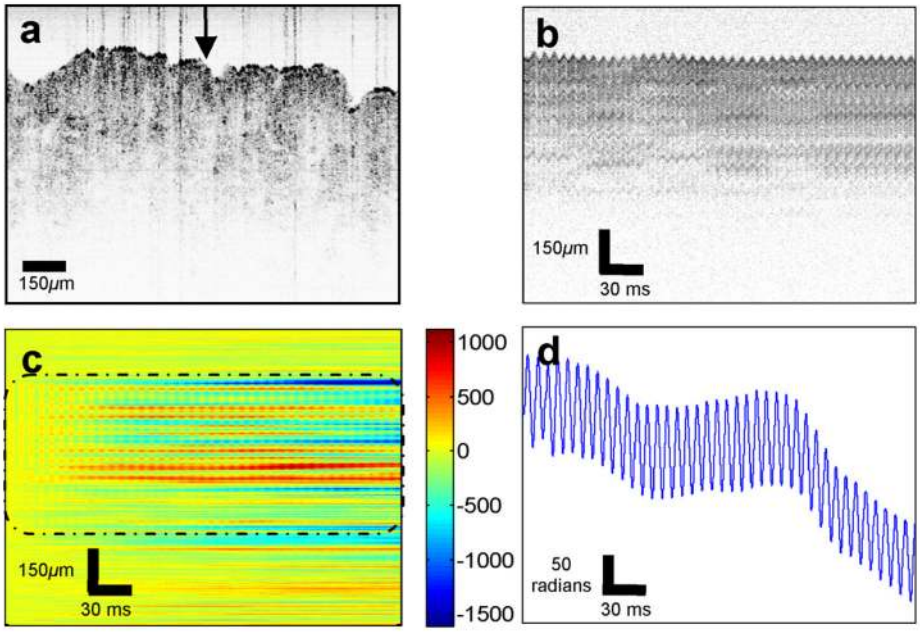

Fig. 4.

OCE images of skin measurement. (a) B-mode OCT image. (b) Amplitude data of M-mode OCE image at the position of arrow in (a). (c) Phase data of M-mode OCE image at the position of arrow in (a). (d) Averaged phase data from the dotted line range in (c). Unit for the color bar is radians.

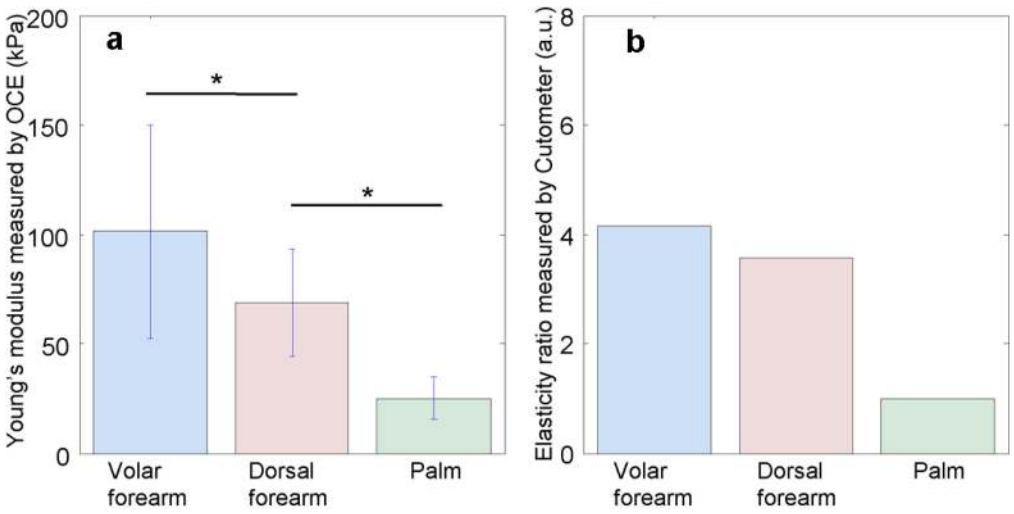

Fig. 5.

Young's moduli measured by OCE from different skin sites with corresponding Cutometer results. (a) Young's moduli of skin on volar forearm, dorsal forearm, and palm. Driving frequency is 50 Hz and measurements were done orthogonal to Langer's lines. (b) Corresponding Cutometer results using the parameter Ur/Uf. Symbol "*" denotes $p < 0.05$.

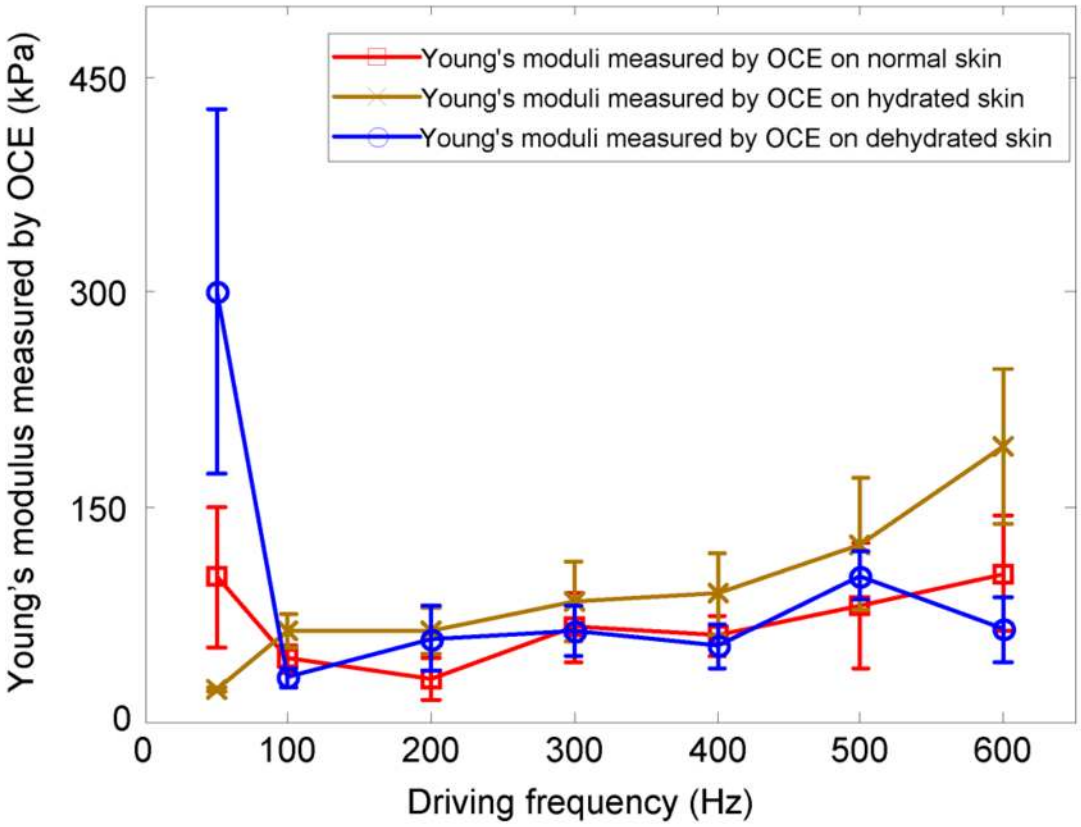

Fig. 6.

Young's moduli measured by OCE under different driving frequencies and skin hydration conditions. Blue line denotes results from dehydrated skin, brown line denotes results on hydrated skin, and red line denotes results on normal untreated skin.

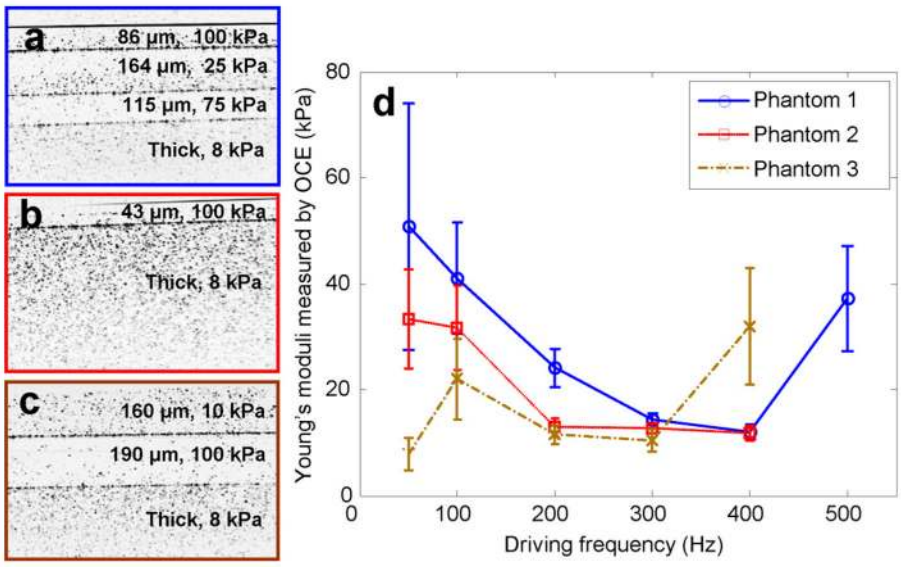

Fig. 7.

Young's moduli measured by OCE under different driving frequencies on three skin tissue phantoms. (a) B-mode OCT image of four-layer phantom 1. (b) B-mode OCT image of two-layer phantom 2. (c) B-mode OCT image of two-layer phantom 3. Each image shows approximate layer thickness and Young's moduli. (d) Young's moduli measured by OCE under different driving frequencies on phantoms 1, 2, and 3.

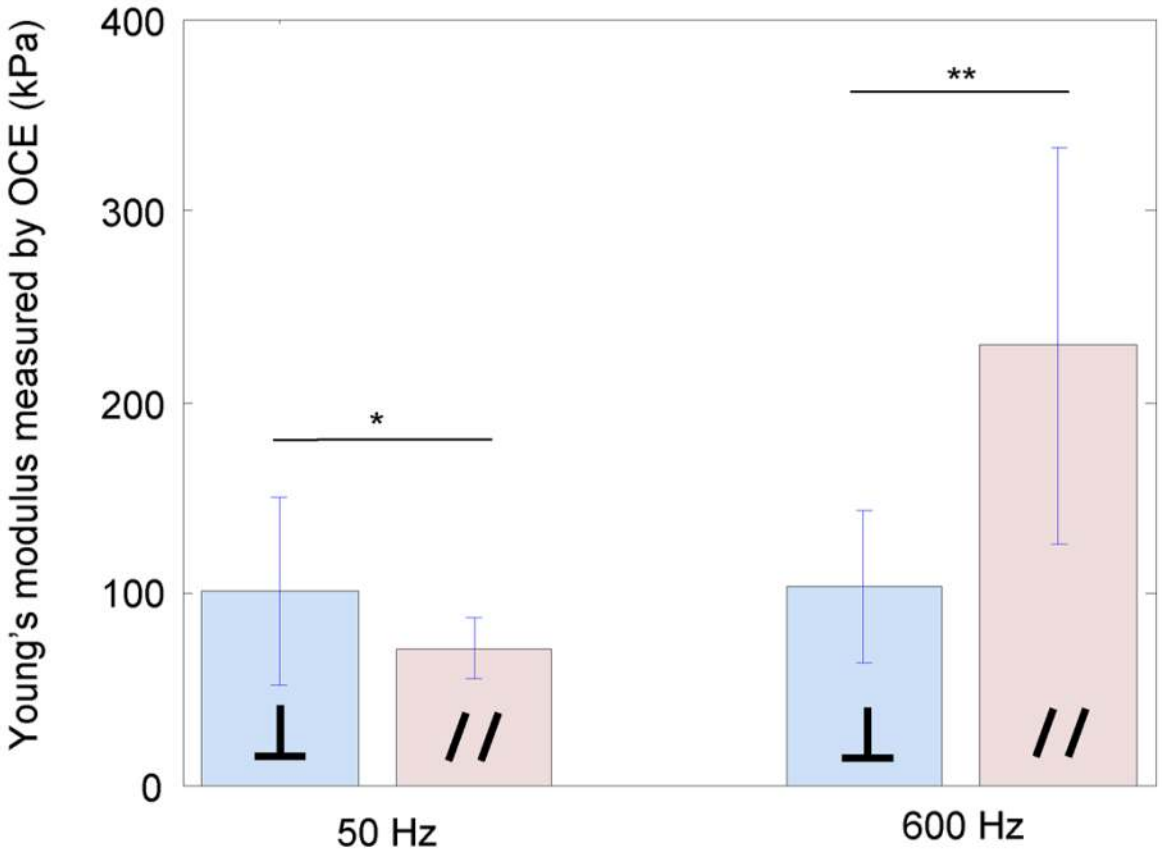

Fig. 8.

Young's moduli measured by OCE from different skin directions under 50 and 600 Hz driving frequencies. The symbol // denotes direction parallel to Langer's lines and ⊥ denotes direction orthogonal to Langer's lines. Symbol "*" denotes $p < 0.05$ and "**" denotes $p < 0.0001$.